International Journal of Pressure Vessels and Piping 179 (2020) 104029

Contents lists available at ScienceDirect

International Journal of Pressure Vessels and Piping

journal homepage: http://www.elsevier.com/locate/ijpvp

Numerical simulation of high-temperature creep deformation in Zr-2.5%Nb pressure tubes of CANDU reactors

Santiago F. Corzo *, Damian E. Ramajo

CIMEC Centro de Investigación de Métodos Computacionales, UNL, CONICET, FICH, Col. Ruta 168 s/n, Predio Conicet "Dr Alberto Cassano", 3000, Santa Fe, Argentina

ARTICLE INFO

Keywords:
Creep
Pressure tube
Nuclear reactor
OpenFOAM®

ABSTRACT

The present paper deals with the development of a numerical approach to predict thermal creep in pressure tubes of CANDU nuclear power reactors. This phenomenon plays a crucial role under accident conditions, where the core can reach high temperature and the pressure tubes can suffer thermal creep with important radial deformation usually named "Ballonning". The Balloning strain in CANDU pressure tubes is a difficult issue from the mathematical point of view due to the visco-plastic nature of the deformation, and the material properties of the tubes, which are made of a Zr–2.5%Nb alloy that presents micro-structural phase change at temperatures close to 800°C. For this reason, an explicit strategy was implemented in OpenFOAM-5.0® assuming the uniaxial deformation in radial direction, neglecting the rotational strains. The proposed model is assessed by reproducing experimental tests before to be applied to model the response of CANDU pressure tubes under Station Blackout and Loss Of Coolant Accident conditions.

1. Introduction

The creep of metallic materials is the plastic deformation promoted by the application of mechanical stress below the yield strength value for a long time. The creep is caused by the movement of dislocations through the micro-structure, the ageing of the micro-structure, and the grain-boundary cavitation [1]. The creep phenomenon takes place in many industrial applications, although it is more frequently found on mechanical pieces subjected to high temperature (close to the melting point) (see Fig. 1).

In nuclear installations there are many critical components affected by creep. In particular, the CANDU (Canadian Deuterium Uranium) nuclear power plants (NPP) are pressure tube type reactors which contain 380 coolant channels disposed horizontally inside a Calandria vessel. The coolant channels house the fuel assemblies, which transfer the fission heat to the heavy-water coolant flow. Inside the channels the coolant is heated from 260°C up to 300°C approximately. There are four inlet headers and four outlet headers disposed around the Calandria to distribute and collect the cold and hot coolant. Each coolant channel is connected to one inlet header and one outlet header through two small diameter tubes named feeders. The primary coolant circuit is divided in two loops, each one contains two steam generator and two main pumps. The loops are linked to each other through the pressure-inventory control system (pressurizer). However, they can be isolated one each other during an emergency event. Fig. 3 illustrates the main components of a CANDU NPP. More details are available in https://canteach.candu.org/.

Each coolant channel is composed of a pressure tube (PT) surrounded by a Calandria tube (CT). Both tubes are concentrical and separated by an annular gap for thermal isolation. The gap is filled with low-pressure carbon dioxide or nitrogen gas. Under normal conditions the PT supports high pressure and temperature conditions (~10MPa and ~300°C) while the CT is subjected to lower pressure and temperature conditions (~0.2 MPa and ~60°C). Therefore, the PT has a higher thickness than the CT. The PT and the CT are made of Zirconium 2.5%*Nb* and Zircaloy-2, respectively. Fig. 2 shows a cross cut sketch of the coolant channel. As shown four garter springs are disposed in order to hold the gap between the PT and the CT. In order to absorb the thermal dilatation in the axial direction a sliding support is place at one side of the PT and CT.

During the plant life operation the slight deformation of the PT caused by creep and sagging (the tube flexes down by own weight and the weight of the fuel bundle) is continually monitored. Nevertheless, under certain abnormal events, such as Loss of Coolant Accident (LOCA) [3–5], and Station Blackout (SBO) events [6–8], the heat-up of the PT

* Corresponding author.
E-mail address: scorzo@santafe-conicet.gov.ar (S.F. Corzo).
URL: http://www.cimec.org.ar (S.F. Corzo).

https://doi.org/10.1016/j.ijpvp.2019.104029
Received 8 March 2019; Received in revised form 4 December 2019; Accepted 5 December 2019
Available online 12 December 2019
0308-0161/

List of symbols

t	Time
$\mathbf{u}$	Displacement vector
ε	Strain tensor
σ	stress tensor
ρ	density
$\mathbf{f}$	Body force
$\mathbf{D}(\varepsilon) = 2\mu\varepsilon + \lambda tr(\varepsilon)\mathbf{I}$	Isotropic elasticity tensor
I	Unit tensor
μ,λ	Lame's coefficients
E	Young's modulus
ν	Poisson's ratio
T	Temperature
$\mathbf{S_f}$	Surface of faces
V_p	Cell volume
f^*_{exp}	Explicit terms
α,β	Micro-structural phases
creep	Creep term
0	Initial
P	Owner cell
f	Face
n	Current time step
$n-1$	Previous time step
CANDU	Canadian Deuterium Uranium
CT	Calandria tube
CV	Control Volume
ECCS	Emergency Core Cooling System
FEM	Finite Element Method
FVM	Finite Volume Method
GAMG	Geometric Algebraic Multi-Grid
IAEA	International Atomic Energy Agency
LOCA	Loss Of Coolant Accident
LRV	Liquid Relief Valves
NPP	Nuclear power plant
OpenFOAM	Open Field Operation and Manipulation
PHTS	Primary Heat Transport System
PT	Pressure tube
RIH	Reactor Inlet Headers
SBO	Station Blackout
SG	Steam Generator

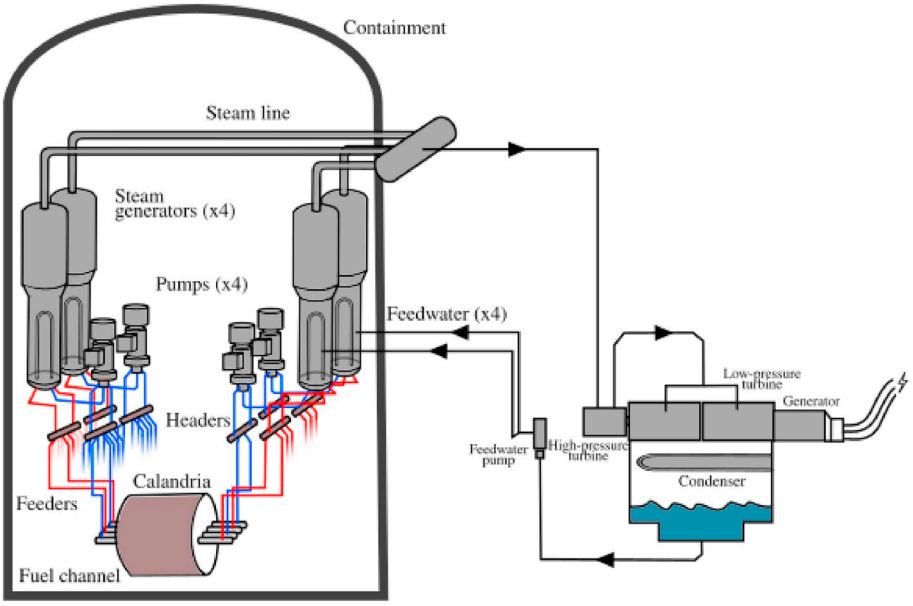

Fig. 1. Sketch of CANDU nuclear power plant.

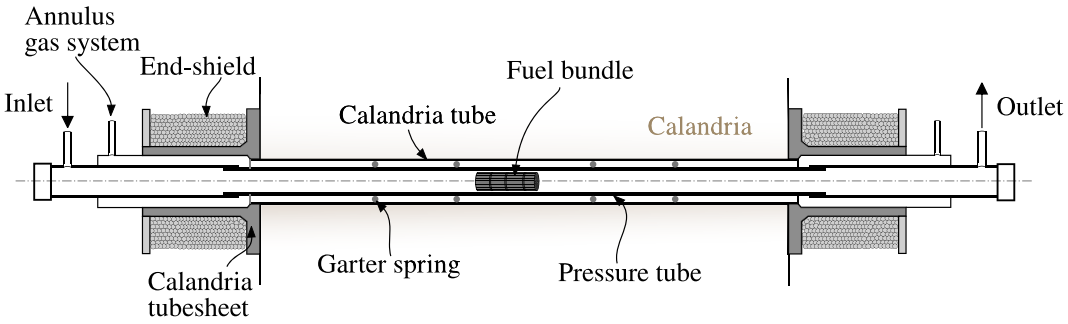

Fig. 2. CANDU coolant channel details.

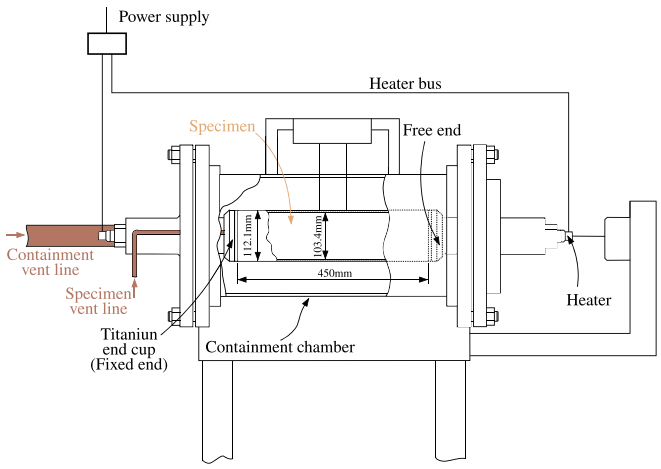

Fig. 3. Experimental facility of Riznic et al. Riznic and Macdonald [2].

could induce excessive creep deformation in radial direction. This is named ballooning and is caused by the application of high internal pressure and temperature. These accident scenarios could have different transient evolution. For instance, during a LOCA the reduction of coolant flow through the channel should increase the temperature of the PT while the pressure is reduced significantly. Both effects are in opposition from the creep-deformation point of view. On the other hand, under a SBO where the main pumps shut-down, the forced flow is lost. Therefore, the heat removed in the steam generators is drastically reduced, and the coolant heats up to reach saturation [9]. Despite the coolant temperature will be lower than in LOCA, the primary system will remain at a pressure higher than in normal operation. Consequently, a SBO event could lead to favorable conditions for creep deformation and ballonning.

The numerical simulation of long-time ballonning deformation in large domains represents a complex problem from the mathematical point of view for two reasons: deformation could take place in the viscous-plastic zone, and the mechanism of deformation is promoted by creep. Another issue is found in the micro-structure phase change from α to β, which takes place around 800°C for Zr–Nb2.5% causing a strong change of the mechanical properties. Due to that, up to day the calculus of ballonning deformation is mainly performed with empirical or semi-empirical correlations, which need for a set of setting parameters obtained from experiments.

Perhaps the widely known model for creep deformation in PT is the empirical correlation proposed by Shewefelt et al. [10], which allow estimating the creep deformation rate for different hoop stress conditions in a broad range of temperatures, and also considering the micro-structure. Shewefelt et al. [11] also analyzed the sagging deformation at high temperature. Combining both models it is possible to have an averaged estimation of the creep and sagging deformations of the PT. More recently, Majumdar et al. [12] proposed an one-dimensional (1D) model to estimate the PT deformation by ballonning and sagging under different thermal conditions and internal pressures. They concluded that, at high pressure the ballonning is the only responsible of the PT to CT contact, while at low pressure and high temperature (LOCA conditions) the sagging deformation becomes relevant.

The numerical simulation of visco-plastic creep deformation, with strain and stress states changing in time, as a consequence of external load and temperature, is a complex task. Examples of these changes include progressive deformation, relaxation and redistribution of stresses, and local reduction of strength. Furthermore, the strain and stress states are in most of cases non-homogeneous and multiaxial [13], which largely increase the numerical cost and difficulty of the solution. On the other hand, in many cases the stress state can be considered uniaxial. Then, it is very convenient to introduce a inelastic strain by creep, ε_{pl}, calculated as the difference between the measured strain ε and the calculated elastic strain ($\varepsilon = \varepsilon_{pl} + \varepsilon_{el}$) [13]. The last converts the problem into a linear-equations system similarly to an initial strain state [14]:

$$\boldsymbol{\sigma} = \mathbf{D}(\varepsilon - \varepsilon_0) \tag{1}$$

where **D** is the isotropic elasticity tensor, and ε_0 is the initial strain. Some authors ([15,16]) have applied successfully this approach in plastic visco-deformation problems. In the current problem the creep dominates in the plastic deformation stage. Hence, the stress effort is applied uniformly in the inner surface of the PT, and creep occurs only in the radial direction. Under these conditions, and without rotational strain, the problem can be suitably solved with this simple approach.

In this paper a three-dimensional (3D) computational model to estimate ballonning deformation in PT is proposed and developed into the Finite Volume Method (FVM). The model is based on a pseudo-elastic model, which incorporates the Shewefelt correlation in an explicit form. The 3D nature of the model allow introducing real thermal stratification conditions within the PT in order to obtain a more accurate description of local deformation. The proposed model is firstly assessed by reproducing experimental tests before to be applied to study the deformation of a PT in CANDU reactor under SBO and LOCA events.

2. Mathematical formulation

The differential form of the solid strain equation defined in terms of balance of forces is:

$$\nabla \cdot \sigma + \rho \mathbf{f} = 0 \tag{2}$$

where σ is the stress tensor, ρ is the density, and **f** is the body force. The strain tensor ε can be defined in terms of the displacement vector **u** as read:

$$\varepsilon = \frac{1}{2}\left[\nabla \mathbf{u} + (\nabla \mathbf{u})^T\right] \tag{3}$$

Then, for pure elastic deformation the Hook's law defines the relationship between the stress and the strain tensors:

$$\sigma = \mathbf{D}(\varepsilon) = 2\mu\varepsilon + \lambda tr(\varepsilon)\mathbf{I} \tag{4}$$

where *I* is the unit tensor, and μ and λ are the Lame's coefficients related to the Young's modulus *E* and the Poisson's ratio *ν*.

However, due to the visco-plastic nature of the deformation, the elastic Hook's law is not proper. Instead of this, an empirical strain rate model, accounting for the combination of creep, dilatation, and α-β phase change, should be added to the right hand side in Equation (2) ($\sigma_{creep} = \mathbf{D}(\varepsilon_{creep})$). Using Equation (3) to rewrite Equation (4) in terms of the displacement vector **u**, the governing Equation (2) reads

$$\nabla \cdot \left[\mu \nabla \mathbf{u} + \mu(\nabla \mathbf{u})^T + \lambda \mathbf{I} tr(\nabla \mathbf{u})\right] = -\rho \mathbf{f} + \nabla \cdot \sigma_{creep} \tag{5}$$

For numerical convenience Equation (5) can be transformed into a semi-explicit form by writing explicitly the sources in the left hand side:

$$\nabla \cdot [(2\mu + \lambda)\nabla \mathbf{u}] = -\rho \mathbf{f} - \nabla \cdot \left[\mu(\nabla \mathbf{u})^T + \lambda \mathbf{I} tr(\nabla \mathbf{u}) - (\mu + \lambda)\nabla \mathbf{u}\right] + \nabla \cdot \sigma_{creep} \tag{6}$$

The creep stress tensor σ_{creep} is obtained by replacing the creep strain ε_{creep} in Equation (4). In this work ε_{creep} is obtained through an explicit approach:

$$\varepsilon^n_{creep} = \varepsilon^{n-1}_{creep} + \dot{\varepsilon}_{creep}\Delta t \tag{7}$$

where n and $n-1$ indicate the current and previous time steps, and the creep strain rate $\dot{\varepsilon}_{creep}$ is estimated by the correlation proposed by Shewfelt et al. Shewfelt et al. [10]; which is based on uniaxial creep tests

for Zr-2.5%Nb:

- For 450°C ≤ T ≤ 500°C

$$\dot{\varepsilon}_{creep} = 1.3 \times 10^{-5} \sigma^{9} exp(-36600 / T) \quad (8)$$

- For 500°C < T ≤ 700°C

$$\dot{\varepsilon}_{creep} = 1.3 \times 10^{-5} \sigma^{9} exp(-36600 / T) + 5.7 \times 10^{7} \sigma^{1.8} exp(-29200 / T) \quad (9)$$

- For 700°C < T ≤ 850°C

$$\dot{\varepsilon}_{creep} = 1.3 \times 10^{-5} \sigma^{9} exp(-36600/T) + \frac{5.7 \times 10^{7} \sigma^{1.8} exp(-29200/T)}{\left[1 + 2.0 \times 10^{10} \int_{t_1}^{t} exp(-29200/T) dt\right]^{0.42}} \quad (10)$$

- For 850°C < T ≤ 950°C

$$\dot{\varepsilon}_{creep} = 10.4 \sigma^{3.4} exp(-19600/T) + \frac{3.5 \times 10^{4} \sigma^{1.4} exp(-19600/T)}{\left[1 + 274 \int_{t_2}^{t} exp(-19600/T)(T-1105)^{3.72} dt\right]} \quad (11)$$

- For 950°C < T ≤ 1200°C

$$\dot{\varepsilon}_{creep} = 10.4 \sigma^{3.4} exp(-19600 / T) \quad (12)$$

where T is the temperature and σ the stress computed in terms of the internal pressure in the PT Majumdar et al. [12].

Summarizing, Equation (6), writing in terms of the displacements **u**, is solved to obtain the deformations, calculating the stress creep ($\sigma_{creep} = \mathbf{D}(\varepsilon_{creep})$) explicitly by the Shewfelt correlations.

In the follow section 2.1, the numerical details about the model implementation and coding are presented.In the developed model, the temperature distribution in the solid can be calculated numerically (solving the energy equation) or imposed in the domain with a time and spacial expression. In the assessed problems in section 3, the temperature distribution was imposed with polynomial equations T(t,x).

2.1. Numerical implementation

A segregated *FVM* numerical scheme was chosen to implement the above described model. That means, the displacement components are sequentially and iteratively solved inside the linear algebraic equations system. The *FVM* is second-order accuracy due to the non-linear governing equation writing in the integral form is solved iteratively. That leads to a diagonal dominant matrices system, which is well suited for iterative solvers.

Equation (6) was implemented into the elasticity solver "elasticSolidFoam" [17] within the suite OpenFOAM-5.0® (Open Field Operation and Manipulation). The use of the elasticSolidFoam solver will allow us to couple this with many other fluid solvers available in OpenFOAM® to simulate single and multi-phase fluid flows, incompressible and compressible flow, thermal flow, etc.

In OpenFOAM® the partial differential equations system is transformed into an algebraic system by applying spatial and temporal discretization. In *FVM* the domain is divided in cells, named Control Volume (*CV*). Each *CV* has a centroid *P*, and is bounded by a set of faces (*f*). The faces can be internal faces, if they are shared by two *CV*, or can be boundary faces when they are in the boundary of the domain. The cells surrounding a *CV* are called neighbors (*N*).

The governing equations have to be satisfied in an integral form in each *CV*. The divergence terms in the *CV* are calculated as the net fluxes through the faces *f* by applying the Gauss theorem, leading to the following expression:

$$-\sum_{f}(2\mu + \lambda)\mathbf{S_f}\cdot(\nabla \mathbf{u}^{n})_{f} = V_P f_P + f^{*}_{exp} \\ -\sum_{f}(2\mu)\mathbf{S_f}\varepsilon_{creep} + \lambda \mathbf{I}\varepsilon^{T}_{creep} \quad (13)$$

where f^{*}_{exp} represents the explicit terms (right hand side of Equation (6)). Note that the fields are constant inside each *CV*. That means, the volume integral of a field is written in terms of the product of the field evaluated in *P* and the volume of the cell, V_P. The algebraic equation (13) is assembled in the displacement matrix for all the *CV*. Then, the resulting linear system can be solved with an iterative solver. Inside the OpenFOAM® background, the algorithm implementation of Eqn. (13) is coded in a simple form:

Displacement matrix in OpenFOAM®s

```
fvVectorMatrix DEqn
    (
    - fvm:: laplacian(2*mu + lambda, D, "laplacian(DD,D")+ fvc:: div(2.0*mu*
    (epsCREEP) + lambda*(I*tr(epsCREEP))) =  = divSigmaExp
    );
```

The main advantage of the *FVM* over the broadly used Finite Elements Method (*FEM*) in solid mechanics simulation is the lower cost of the iterative solvers instead of the direct methods usually used for solving the large matrices generated with *FEM*. On the other hand, a disadvantage of *FVM* is the lower order of precision get for the same mesh, and the necessity of iterate over the explicit cross-component coupling [17].

Other code implementations were required in the solver like the coding of Shewfelt correlation (Eqns. (8)–(12)) to compute ε_{creep} for each CV in Eqn. (13). The energy equation in the solver "elasticSolidFoam" is calculated in term of the temperature (*T*). Once the solver was coded and compiled, the setting of a new problem is similar like any other solver. The user must to define the initial and boundary conditions into the "initial condition" directory for the displacement vector *u* and the temperature *T*, the numerical settings in the "system" directory and the physical parameters added to the mesh in the "constant". More details are available in the OpenFOAM® documentation (www.openfoam.org).

External sources can be included in the problem setting with the "fvOptions" libraries for both fields *u* and *T*. The user can define an analytical expression for the temperature in terms of time and position. This feature was used in the reported tests to impose the thermal condition.

3. Results and discussion

3.1. Homogeneous deformation tests

The PT experimental facility results published by Riznic and Macdonald [2] were chosen to assess the current code implementation. Fig. 3 shows a sketch of the test consisted of a PT of 450 mm length, and inner and outer diameters of 103.4 mm and 112.1 mm, respectively. The PT is made of Zr-2.5%Nb and housed inside a containment chamber.

The PT was homogeneously heated around the circumferential direction by electrical induction with a heating rate of 35° C/s. The inner side of the PT was pressurized with steam. Nine tests were carried out for different pressure and temperature conditions. In this paper the highest pressure test (F-286) at 6 MPa was choice for validation.

The domain was meshed with 210,000 structured hexahedral cells.

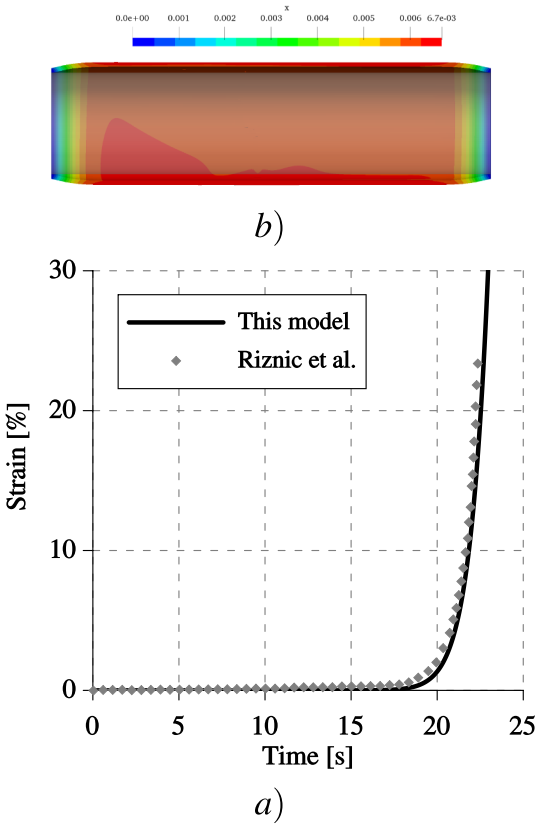

Fig. 4. Computational results: a) Strain vs time of the test F-286, b) Deformation at 22 s.

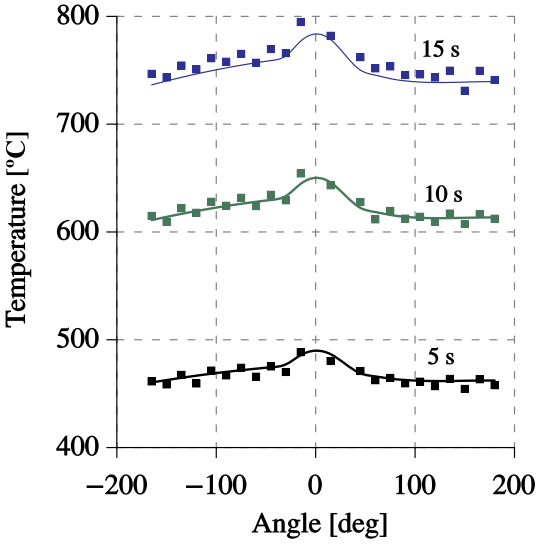

Fig. 5. Circumferential temperature distribution.

Both PT ends were radially constrained whereas the inner and outer walls were free to move. The homogeneous heating was imposed as an energy volume source. A constant time step of 0.05s was suitable for simulations. The Geometric Algebraic Multi-Grid (GAMG) method was selected to solve the deformation linear equation. The tolerance criteria for the linear solver was an absolute residual of 10^{-9}, or a relative residual of 10^{-2}. The material properties were extracted from literature. For the elastic modulus (E), a linear dependency with temperature was adopted ($E(T) = 95.9 - 0.0574T[^{\circ}C]$, [GPa]) Allen [18].

Fig. 4-a shows the mean strain in the radial direction. As noted the numerical results are in very good agreement with the experiment data until to reach the tube failure at 22.5s. The failure prediction is not considered in the current computational model. In Fig. 4-b the PT deformation at 22 s is displayed. As can be see the homogeneous ballooning deformation is in the whole tube, excepting at both ends, where it is radially constrained.

3.2. Non-homogeneous deformation tests

To demonstrate the potentiality of the code to predict non-homogeneous deformation, the experiment performed by Forrest [19] was reproduced. In this case the specimen, the inner pressure and the heating rate were the same than for the previous test. On the other hand, the heating was non-homogeneous in the circumferential direction, but it was uniform along the axial one. Fig. 5 shows the circumferential distribution of temperature measured at three times. The dots corresponds to measured data, and the lines are fitting curves to feed the simulations.

For this case the simulation lasted 16 s, which was more than the 15.7 s to reach the failure. Fig. 6-a shows the PT deformation predicted by the model at three times. Clearly, the deformation is non-uniform due to the temperature distribution imposed. The mean strain and mean temperature are drawn in Fig. 6-b. Different from the previous case for homogeneous heating (see Fig. 4-a) where slight deformation was found before 15*s*. In the current case the deformation started at 10*s*. The comparison with experimental data (dots in Fig. 6-b) allow concluding that the computational model is also able to predict creep deformation caused by non-homogeneous temperature fields, which can be produced by the two-phase flow stratification inside horizontal PT of CANDU reactors during an accident event.

As noted in Fig. 6-b, the mean temperature never overcame the phase-change $\alpha - \beta$ onset ($850^{\circ}C$). Three deformation regions can be identified as I, II, and III in this figure. In region I, before 6*s*, the temperature keeps lower than $500^{\circ}C$, and creep deformation is negligible. In region II, the temperature is higher than $500^{\circ}C$ and the dislocations in the micro-structure of the material begin to align. Consequently, the strain increases up to 3%. Despite of that, at the first part of region II the creep deformation remains small, which is expected from PT design. In region III ($T > 700^{\circ}C$), the strain displays a power law behavior, as indicated by Equation (10) where the deformation increment is largely higher than region II. The large deformation of 20% at temperatures below the phase change temperature ($< 500^{\circ}C$), is a consequence of the high inner pressure. This situation is expected under SBO events, for which the pressure increases over the normal operation while the temperature remains lower than the high values expected in LOCA.

Fig. 7 shows three views of the deformed PT at 16s. Despite of the prediction of PT failure is unable with the current model, the position of the failure would be identified considering that experimental visualization locate the break in the largest deformation zone (See Fig. 7).

Many severe accident codes for nuclear safety assume that the PT/CT break at high pressure is reached once a fixed onset temperature is overcome. Based on the experimental evidence, this simple criteria seems to be appropriated; The high forces in the inner surface of the PT trigger the large deformations, and consequently the break.

3.3. Station Blackout accident simulation

The SBO accident consists of the loss of the main and auxiliary electric supplies (commonly Diesel generators). Under this condition, the main systems are losses: Primary pumps, heaters of the pressurizer, feed-water pumps of the secondary system, etc. Although the reactor is immediately shut-down, the loos of forced convection added to the core decay power (around 5% of the nominal power) slowly increases the temperature and pressure in the primary heat transport system (*PHTS*). Once the water in the steam generators (*SG*) is completely evaporated,

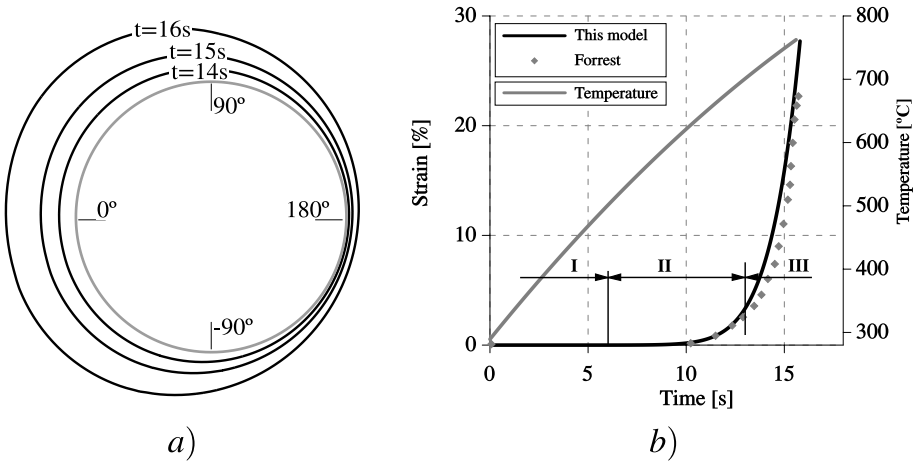

Fig. 6. Computational results: a) Contours of radial deformation at four times, b) Mean strain (%) vs time.

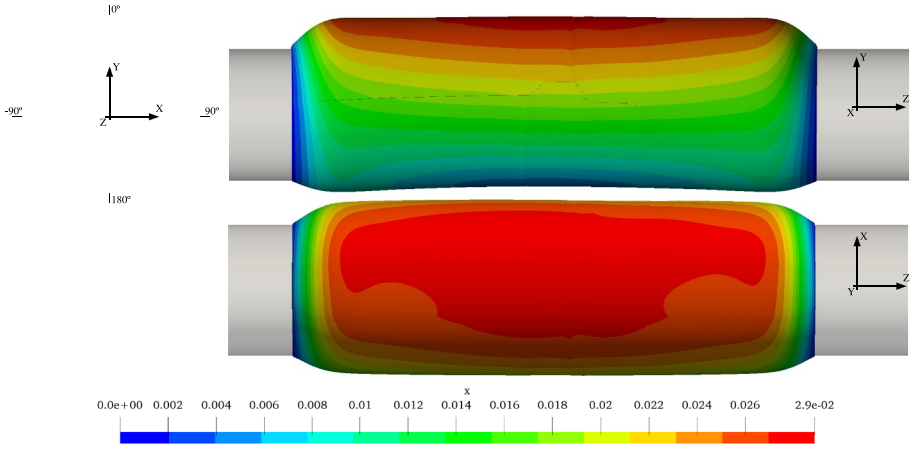

Fig. 7. Tube deformation at 16s.

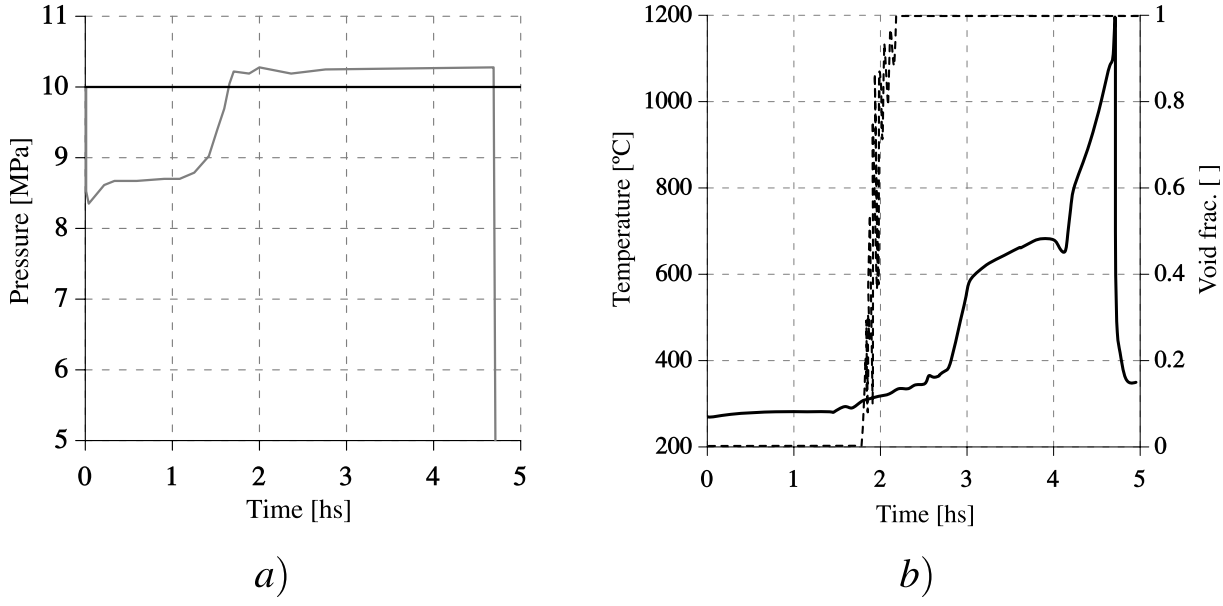

Fig. 8. Station Blackout accident TECDOC-1727 [20]: a) Pressure in the *PHTS*, b) Temperature and void fraction in the *PHTS*.

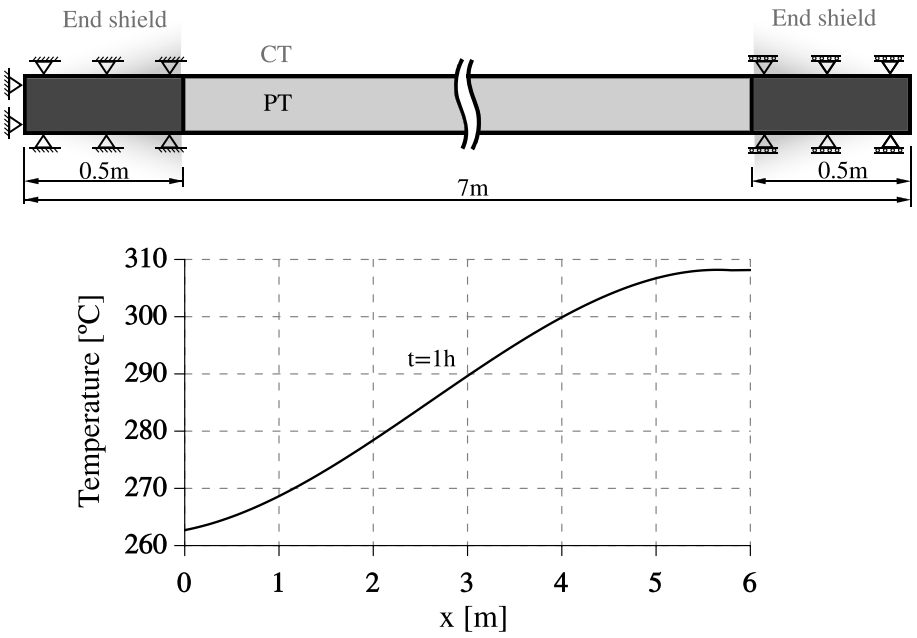

Fig. 9. Top: Domain geometry. Bottom: Temperature axial profile at 1 h after SBO was initiated.

the pressure in the *PHTS* increases up to reach the Liquid Relief Valves (*LRV*) set point.

The CANDU-6 NPP response under a SBO accident was reported by the International Atomic Energy Agency (IAEA) TECDOC-1727 [20]; based on the predictions of many simulation codes finding a general agreement about the main sequences of the event.

According with the IAEA report TECDOC-1727 [20]; the main events in the first stage of the SBO accident (before *PHTS* blow-down) can be summarized as follow:

1. The reactor is shut-down.
2. The turbine trip takes place due to the loos of the power supply.
3. In the secondary system the steam is relief through the Main Steam Safety Valves: The natural convection in the *PHTS* guarantees the decay heat removal meanwhile the *SGs* inventory in not completely lost. The temperature and pressure in the *PHTS* reduces due to the high heat transferred in the *SGs*.
4. The steam generators inventory depletion takes place around 2hs after the event initiated. Hence, the heat removal from the PHTS decays and the coolant pressure increases.
5. The Liquid Relief Valves (*LRV*) open due to high pressure in the *PHTS* (10.24 MPa): It is expected that the coolant be discharged into the containment building rather than into the degasser condenser. The loss of coolant through the *LRVs* continues until to the fuel channel dryout is reached.
6. The moderator inventory is the only heat sink available. It is gradually boiled and the liquid level in the Calandria vessel decreases due to the decay heat.
7. 5 hs after SBO initiated the heatup at high pressure induces the PT ballooning, and next the rupture of the PT and the CT tubes, causing a fast blow-down from the *PHTS* into the Calandria vessel.

The moderator fluid inside the Calandria represents a significant heat sink to delay the PT/CT breaks because the PT/CT contact disrupts the gap isolation and increases the heat transfer from the *PTHS* to the moderator. In this sense, to predict how many PT/CT put in contact by ballooning is of great importance. In this section, the temperature and pressure evolution extracted from TECDOC-1727 [20] for SBO events are applied to the PT model to predict the PT/CT contact.

Fig. 8 shows the evolution of pressure, temperature and void fraction in the *PTHS* during a SBO. More details of these results was presented in TECDOC-1727 [20].

Table 1
Geometric details of the CANDU-6 fuel channel.

Description	Value
Fuel channel length	5.944 m
Pressure tube outer diameter	0.112,064 m
Pressure tube wall thickness	0.004343 m
Calandria tube outer diameter	0.1317 m
Calandria tube wall thickness	0.0014 m

Due to the rapid reactor shutdown system, the pressure fall down in the first seconds and it remains less than 8.7 *MPa* during the first hour. The temperature also remains constant during the first 2 h after the *SGs* lost all the inventory. Next, the coolant evaporation starts and the temperature and pressure increase abruptly.

Before to the channel dryout the PT temperature remains almost constant around the saturation conditions. After that, the temperature increases quickly while the pressure is kept almost constant due to the action of the *LRV*. Finally, the PT/CT breaks after 4.5 hs and the moderator fills the PT.

In the current PT analysis the reduction of pressure during the first 2.5 hs, before *SG* inventory depletion (item 4 in the event sequence), was neglected, and a constant pressure of 10*MPa* was assumed (See Fig. 8-a). Regarding temperature, the mean averaged temperature showed in Fig. 8-b was imposed in the domain. The domain geometry is shown in Fig. 9 at the top. The dimensions are summarized in Table 1. This was meshed with 181,120 cells. The left end was fixed embedded, and the right end was free to move in the axial direction. Such as in the real fuel channels, the PT was extended 0.5 m at both ends inside the end-shields to consider the mechanical restriction imposed by the embedded. To achieve more realistic simulations, the mean averaged temperature in Fig. 8-b was imposed by considering the axial temperature profile displayed in Fig. 9 at the bottom. This profile correspond to the coolant temperature 1 h after the SBO was initiated.

Certainly, the temperature averaged in the axial direction coincides with the temperature showed in Fig. 8-b for 1 h. As noted, the highest temperature is in the PT outlet. Therefore, it is expected that ballonning initiate at the right and extend to the left side. This is displayed in

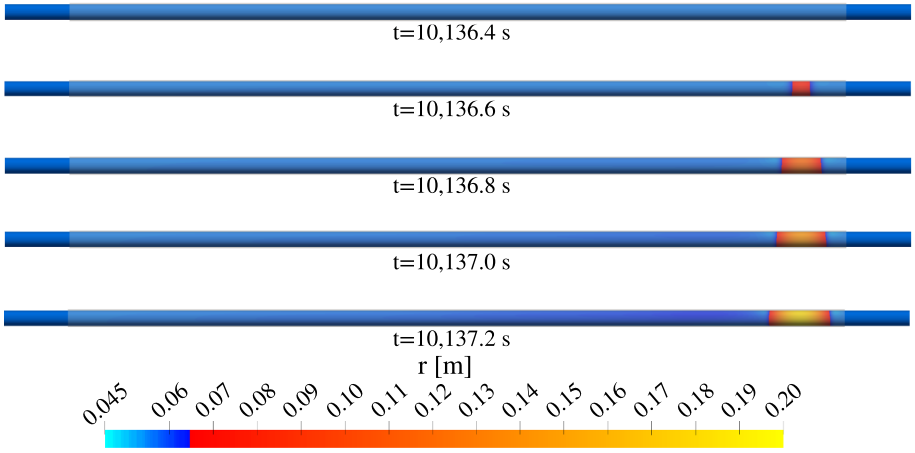

Fig. 10. Evolution of the radius of the PT during the Station Black-Out accident.

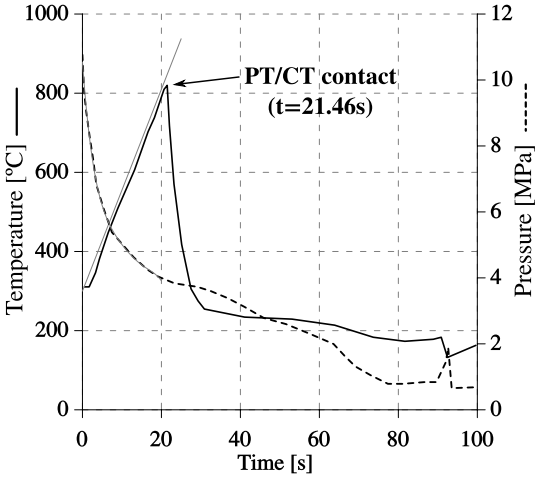

Fig. 11. Inner pressure and temperature of the pressure tube for the Loss Of Coolant Accident Oh et al. [5].

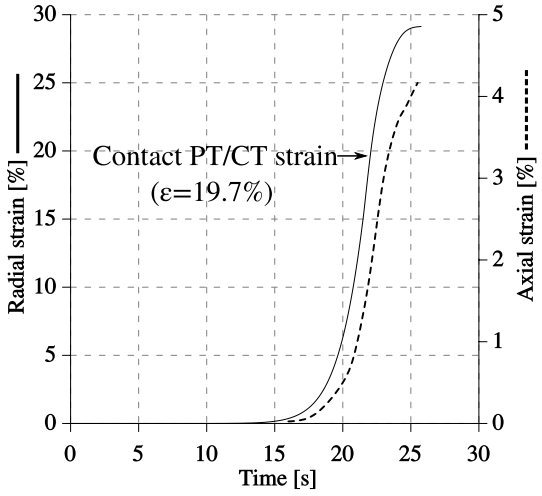

Fig. 12. Radial and axial strain of the pressure tube for the Loss Of Coolant Accident.

Fig. 10, where the radius of the PT is shown at five times. As noted, once the creep deformation starts (t = 10,136.4 s), it propagated very fast, and the rate of deformation is about one diameter per 0.2 s.

During the first 3*hs* the PT shows slight deformation. After that, the temperature increases quickly from 400°C to 600°C and the thermal creep becomes predominant, at 2hs:50min occurs the PT/CT contact. Like shown in Fig. 10, the ballonning quickly extends to the left. Once ballonning starts, the PT/CT contact in the whole fuel channel should take less than 6 s, which represent a very small fraction of the total simulation time. Due to only the PT is represented in the current model, the simulation was finished once the PT diameter grew beyond the CT diameter, which take place at $t = 10,137.2s$.

3.4. Loss of coolant accident simulation

In contrast to SBO accidents, in LOCA the PHTS suffers a fast depressurization while large amount of coolant is leaked into the contention building. The low pressure enhances the coolant evaporation and the channel dryout is achieved in a short time causing high temperature increments. A commonly analyzed scenario is the break of 35% in one of the reactor inlet headers (RIH), which produces a fast evaporation inside the reactor core. Although the increase of the void fraction leads to a very fast reactor power pulse several times larger than the nominal power, it is quickly extincted by the reactor shut-down system.

Fig. 11 shows the pressure and the temperature distributions reported by Oh et al. [5] in one coolant channel of a CANDU reactor. The pressure inside the PT fall down rapidly and the temperature increases linearly during the first 20*s*. The void fraction (not draw in the graphic) approximates to 1.0 in the first seconds, although the complete evaporation is not reached. Due to the *RIH* break a reversal flow is expected to occur in the coolant channel. However, this is in opposition with the main pump flow leading to the channel flow stagnation after 10*s*. Although the emergency core coolant system is available, it takes more than 80*s* to refill the channel. Before that, the temperature in the fuel rods increases up to 1300°*C*, and the temperature of the PT rises up to 800°*C* in only 21*s* as displayed in Fig. 11. At this short time the PT and CT put in contact enhancing the heat transfer to the moderator. As a consequence, the temperature of the PT is rapidly reduced even below to the normal operation temperature in around 10*s*. It is concluded that, previous to the Emergency Core Cooling System (ECCS) refilling, the integrity of the fuel channel depends on the PT/CT contact. The high heat transfer is guaranteed because on the moderator subcooled temperature added to the large moderator inventory. Due to that, the CT dryout should not be achieved before the core be refilled. The ECCS should maintain the pressure and temperature in safety conditions.

The model setting were the same used for the SBO study. For temperature, uniform distributions along the axial and circumferential directions were extracted from the work of Oh et al. [5] (See gray curve in Fig. 11). Despite the neglect of the axial temperature variations, the flow

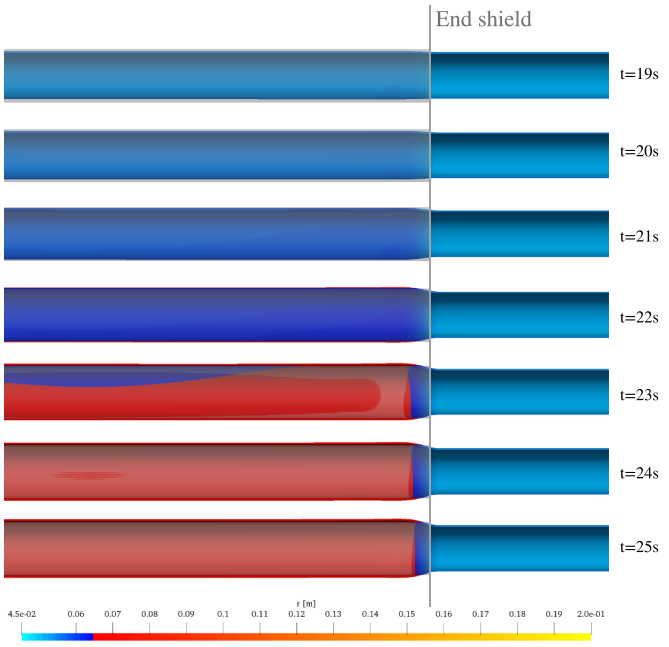

Fig. 13. Radial deformation of the pressure tube for the Loss Of Coolant Accident.

stagnation achieved during the first 10*s* strengthens this assumption. The pressure condition was fitted with polynomial expressions from results of Oh et al. [5] (See Fig. 11).

The simulation time was significantly smaller than for the SBO case because the PT/CT contact was expected to occur before 22s. The radial and axial strain deformations are drawn in Fig. 12. Slightly deformation is observed for temperatures lower than 600°C. On the contrary, once the temperature increases up to 800°C (after 20 s), the strain grows linearly and the PT/CT contact takes place in less than 2*s* for a radial strain of $\varepsilon = 19.7\%$. Note that the axial strain (dashed line) in the right side scale remains around one order lower than the radial strain. However, this axial elongation is proportional to the radial creep and both curves display the same behavior.

For the current model, the variation of the internal pressure has a significant effect in the strain; Beyond 23 s the radial strain begins to reduce until to keep constant, because at pressures lower than 4 MPa the creep deformation becomes very slow. As above mentioned, the current model to predict the radial strain of the PT does not include the mechanical restriction imposed by the CT during the PT/CT contact. However, this model simplification seems reasonable because on the thickness of the PT is four times larger than the thickness of the CT.

Fig. 13 displays the radial deformation in the right end of the PT at seven times from 19 s to 25 s. The color bar is bounded to easy identify the PT/CT contact ($r = 0.06445$ m). The tube deformation is not longer influenced by the End shield restriction. Although the current model does not consider the presence of the three spring separators placed in the gap, the mechanical strength of these components is very small to longer affect the PT/CT contact. At the end of simulation (25 s) the PT/CT contact fulfills the most of the channel, which is advantageous from the safety point of view.

4. Conclusions

In the present paper, the implementation of a computational method to predict creep deformation in CANDU reactor coolant channels is developed. The ballooning deformation associated to high pressure and temperature conditions is responsible of the pressure tube to Calandria tube contact, which largely improves the fuel rods cooling under Station Black-Out and Loss Of Coolant Accident events. The current method allow estimating the contact, which is of significant relevance for nuclear safety.

The comparison with experimental benchmarks showed that the uniaxial radial deformation technique is suitable even for large deformation problems with uniform and non-uniform temperature distributions.

The creep deformation of the real pressure-tube geometry of a CANDU reactor was addressed by considering two extreme situations: the Station Black-Out and the Loss Of Coolant Accident. In both cases, the pressure and temperature conditions extracted from literature were applied and the pressure tube to Calandria tube contact was found. For the Station Black-Out case, the creep deformation was detected after 2.5*hr* while for the Loss Of Coolant Accident case the deformation initiated at 19*s* and the whole pressure tube put in contact with the Calandria tube in only 25 s.

Future works includes the implementation of a contact model to restrict the pressure tube strain, the estimation of the heat transfer by conduction in the contact zone, and the coupling between the current thermal-mechanics model and the thermal-fluid dynamic simulation of the coolant and moderator fluids to introduce more realistic conditions for system code simulations.

Author contribution statement

Corzo Santiago Francisco: Investigation. Damian Enrrique Ramajo: Supervision

Acknowledgements

The authors would like to thank Universidad Nacional del Litoral (CAI + D 2016 PIC 50420150100067LI), Agencia Nacional de Promocion Cientifica y Tecnologica (PICT 2016–2908) and Consejo Nacional de Investigaciones Cientificas y Tecnologicas.

References

[1] D. Askeland, The Science and Engineering of Materials, third ed., *Transparency Masters*. PWS Pub., 1994, 9780534934316.
[2] J.R. Riznic, L.D. Macdonald, Pressure Tube Ballooning Experiments Analysis, 1997.
[3] M. Kim, H.K. Kim, H.J. Kim, S.H. Hwang, I.S. Hong, C.H. Kim, Enhancement of safety analysis capability for a candu-6 reactor using relap-candu/scan coupled code system, Nucl. Technol. 156 (2) (2006) 159–167.
[4] D. Dupleac, M. Mladin, I. Prisecaru, Scdap/relap5 analysis of progression of severe accident in candu 6 plant, in: 17th International Conference on Nuclear Engineering, American Society of Mechanical Engineers, 2009, pp. 47–57.
[5] D. Oh, M. Ohn, K. Lee, Safety Assessment for Loca in Candu Reactor Loaded with Canflex-Nu Fuel Bundles, 1997.
[6] L. Tong, X. Cao, K. Yuan, G. Huang, Severe accident progression analysis induced by station blackout for candu station, Atomic Energy Sci. Technol. 44 (11) (2010) 1361–1365.
[7] S. Petoukhov, Maap4-candu simulation results for candu 6 accident management measure: steam generator secondary side water make-up from dousing tank for the station blackout scenario, in: The 19th Pacific Basin Nuclear Conference (PBNC 2014), 2014. *Vancouver, British Columbia, Canada*.
[8] F. Zhou, D.R. Novog, Relap5 simulation of candu station blackout accidents with/without water make-up to the steam generators, Nucl. Eng. Des. 318 (2017) 35–53.
[9] F. Zhou, D. Novog, Mechanistic modelling of station blackout accidents for a generic 900 mw candu plant using the modified relap/scdapsim/mod3. 6 code, Nucl. Eng. Des. 335 (2018) 71–93.
[10] R. Shewfelt, L. Lyall, D. Godin, A high-temperature creep model for zr-2.5 wt% nb pressure tubes, J. Nucl. Mater. 125 (2) (1984) 228–235.
[11] R. Shewfelt, L. Lyall, A high-temperature longitudinal strain rate equation for zr-2.5 wt% nb pressure tubes, J. Nucl. Mater. 132 (1) (1985) 41–46.
[12] P. Majumdar, D. Mukhopadhyay, S. Gupta, H. Kushwaha, V.V. Raj, Simulation of pressure tube deformation during high temperature transients, Int. J. Press. Vessel. Pip. 81 (7) (2004) 575–581.
[13] K. Naumenko, Modeling of High-Temperature Creep for Structural Analysis Applications, 2018.
[14] O.C. Zienkiewicz, R.L. Taylor, The Finite Element Method for Solid and Structural Mechanics, Elsevier, 2005.
[15] O. Zienkiewicz, I. Cormeau, Visco-plasticity–plasticity and creep in elastic solids–a unified numerical solution approach, Int. J. Numer. Methods Eng. 8 (4) (1974) 821–845.

[16] S. Koric, B.G. Thomas, Thermo-mechanical models of steel solidification based on two elastic visco-plastic constitutive laws, J. Mater. Process. Technol. 197 (1–3) (2008) 408–418.
[17] H. Jasak, H. Weller, Application of the finite volume method and unstructured meshes to linear elasticity, Int. J. Numer. Methods Eng. 48 (2) (2000) 267–287.
[18] G. Allen, Advanced Techniques for the Characterization of Hydrided Zirconium Alloy, Ph.D. thesis, 2011.
[19] C. Forrest, Ballooning of Candu Pressure Tubes-Experiments with Degraded Tube Material. Technical Report, Atomic Energy Control Board, 1995.
[20] TECDOC-1727, Benchmarking Severe Accident Computer Codes for Heavy Water Reactor Applications, Technical Report, IAEA, 2013.